

Static surface mode expansion for the full-wave scattering from penetrable objects

Carlo Forestiere, Giovanni Gravina, Giovanni Miano, Guglielmo Rubinacci, Antonello Tamburrino

Abstract—We introduce the longitudinal and transverse static surface modes and use them to solve the full-wave electromagnetic scattering problem from penetrable objects. The longitudinal static modes are the eigenmodes with zero surface curl of the electrostatic integral operator that gives the tangential component of the electric field, as a function of the surface charge density. The transverse static modes are the eigenmodes with zero surface divergence of the magnetostatic integral operator that returns the tangential component of the vector potential, as a function of the surface current distribution. The static modes only depend on the shape of the object, thus, the same static basis can be used regardless of the frequency of operation and of the material constituting the object. We expand the unknown surface currents of the Poggio-Miller-Chang-Harrington-Wu-Tsai surface integral equations in terms of the static surface modes and solve them using the Galerkin-projection scheme. The static modes expansion allows the regularization of the singular integral operators and yields a drastic reduction of the number of unknowns compared to a discretization based on sub-domain basis functions. The introduced expansion significantly reduces the cpu-time required for the numerical solution of the scattering problem from particle arrays.

Index Terms—Electromagnetic scattering, Eigenvalues and eigenfunctions, Resonance, Resonators, Computational Electromagnetics, Integral Equations, Plasmonics, Dielectric Resonators.

I. INTRODUCTION

The analysis and design of the electromagnetic scattering from a collection of mutually coupled objects is of great importance for many applications, spanning from antenna arrays [1] to metasurfaces [2] and metalens [3]. In this context, the use of integral formulations is appealing, since the unknowns are defined only within the objects' volume or, if the objects are spatially piecewise homogeneous, on their boundary and internal interfaces, while the radiation condition at infinity is naturally satisfied. Nevertheless, the corresponding discrete problem is characterized by dense matrices, and their inversion is usually associated with high computational burden, even when acceleration techniques like fast multipole algorithms are implemented [4].

Accurate and efficient solutions of integral formulations heavily depend on the choice of basis functions. Two macro-categories of basis functions may be identified: *sub-domain*

functions, which are non-zero only over a portion of the object, or *entire-domain* functions, which extend over the entire domain of the object. Although sub-domain functions may have a wider applicability, and are arguably more robust when dealing with objects of irregular shape and sharp corners, entire-domain functions are very appealing when multiple scattering problems are considered, where the electromagnetic system under investigation is a collection of mutually-coupled objects [5], [6], [7].

Representative examples of sub-domain functions are those involved in the divergence-conforming Galerkin method: for instance the Rao-Wilton-Glisson functions [8], loop/star functions [9], [10], [11], [12], loop/tree functions [13], Trintinalia-Ling functions [14], Buffa-Christiansen functions [15], higher order vector basis functions of Nedelec type [16], etc.

Dually, classic examples of entire-domain basis functions are the vector spherical wave functions (see for instance [17]), and the vector spheroidal wave functions [18]. Analytical entire-domain bases may be generated in coordinate systems where the Helmholtz equation is separable. A different but effective strategy to generate entire domain basis functions even in irregular domains is to introduce a convenient auxiliary eigenvalue problem. This is done for instance with characteristic modes [19], [20], [21], [22], (see [5], [6] for arrays of perfectly conductive particles and [23] for perfectly conductive metasurfaces). The characteristic modes do not depend on the particular excitation conditions, and they are effective in the numerical solution of the problems of electromagnetic scattering from collections of objects of given material at a fixed operating frequency. Nevertheless, characteristic modes do depend on the frequency, and their interesting properties are lost if they are used as a basis at a frequency different from the one at which they are computed. Thus, they may not be the best choice when multiple frequencies are involved since they have to be recalculated at each frequency.

In this paper, we introduce a different set of entire domain basis functions that we call “static” surface current modes. These modes are the union of two sets: longitudinal and transverse modes, exhibiting vanishing surface curl and surface divergence, respectively. We assemble these two sets by solving two *auxiliary* frequency-independent eigenvalue problems, involving Hermitian and positive-definite surface integral operators, having the *static* Green's function as kernel. The static modes are the low-frequency limit of the resonance modes of surfaces of finite conductivity [24]. Their volume counterparts have been presented in [25], [26] and in [27] where they have been already used to expand the electromagnetic field [28], [29], [30], [31].

C. Forestiere, G. Gravina G. Miano, G. Rubinacci are with the Department of Electrical Engineering and Information Technology, Università degli Studi di Napoli Federico II, via Claudio 21, Napoli, 80125, Italy

G. Gravina is with 10th Aircraft Maintenance Department, Italian Air Force, Viale dell'Aeronautica 1, 73013 Galatina, Lecce, Italy

A. Tamburrino is with Dipartimento di Ingegneria Elettrica e dell'Informazione “M. Scarano”, Università degli Studi di Cassino e del Lazio Meridionale, Via G. Di Biasio n. 43, 03043 Cassino (FR), Italy

The static modes can be also considered as “high level expansion functions”, belonging to the same categories of the functions introduced in [32], [33], [34], [35], which are typically used in the solution of integral equations in electrically large structure to reduce the number of unknowns. They are not bound to the conventional discretization limit of $\lambda/20$, to which the local basis function discretization is constrained. The proposed basis shares similarities with the one introduced by Vecchi et al. and used in a hybrid spectral-spatial method for the analysis of printed antennas [36], [37].

We demonstrate that the use of the static modes in the Galerkin projection of the Poggio-Miller-Chang-Harrington-Wu-Tsai surface integral formulation [38], [20], [39], [40] leads to: i) a regularization of the scattering integral operator; ii) a drastic reduction of the number of unknowns with respect to sub-domain basis functions without deteriorating the accuracy of the solution; iii) a reduction of the cpu-time required for the solution of multiple scattering problems.

The paper is organized as follows: in Sec. II we introduce the static basis; in Sec. III we recall the Poggio-Miller-Chang-Harrington-Wu-Tsai formulation and we show that the static mode expansion regularizes the involved operator, and that a proper rescaling of the unknowns makes this formulation immune from the low-frequency breakdown. In Sec. IV, we validate the introduced method in two resonant scattering problems, namely the scattering from a metal particle and high-permittivity particle in the visible/near-infrared spectral range. Eventually, we apply this method to the solution of a multiple scattering problem. In Sec. V we draw the conclusions.

II. STATIC SURFACE CURRENT MODES

We denote with Ω a bounded three-dimensional domain, whose boundary $\partial\Omega$ is “sufficiently regular” [41]; $\hat{\mathbf{n}}$ is the normal to $\partial\Omega$ pointing outward. A sufficiently smooth vector field \mathbf{j} defined on a regular surface $\partial\Omega$ can be resolved into the sum of two components [42], [43]: an irrotational and non-solenoidal vector field \mathbf{j}^{\parallel} and a solenoidal and rotational (non zero curl) vector field \mathbf{j}^{\perp} . The vector fields \mathbf{j}^{\parallel} and \mathbf{j}^{\perp} are orthogonal according to the scalar product

$$\langle \mathbf{C}, \mathbf{D} \rangle = \int_{\partial\Omega} \mathbf{C}^* \cdot \mathbf{D} \, dS. \quad (1)$$

In the following, we introduce a basis for each of the two components.

A. Longitudinal static modes

The longitudinal static surface current modes (called in the following *longitudinal static modes* for brevity) are nontrivial solutions of the eigenvalue problem:

$$\mathcal{T}_0^{\parallel} \{ \mathbf{j}_k^{\parallel} \} (\mathbf{r}) = \gamma_k^{\parallel} \mathbf{j}_k^{\parallel} \quad \text{on } \partial\Omega, \quad (2)$$

where

$$\mathcal{T}_0^{\parallel} \{ \mathbf{w} \} (\mathbf{r}) = \hat{\mathbf{n}} \times \hat{\mathbf{n}} \times \nabla \oint_{\partial\Omega} g_0(\mathbf{r} - \mathbf{r}') \nabla'_S \cdot \mathbf{w}(\mathbf{r}') \, dS', \quad (3)$$

and g_0 is the homogeneous space static Green’s function

$$g_0(\mathbf{r} - \mathbf{r}') = \frac{1}{4\pi} \frac{1}{|\mathbf{r} - \mathbf{r}'|}. \quad (4)$$

Apart from a multiplicative factor, the integral operator 3 gives the tangential component of the static electric field generated by a surface charge density distribution. Its spectrum has the following properties (see [25]):

- i the eigenvalues $\{\gamma_k^{\parallel}\}$ and the corresponding eigenmodes $\{\mathbf{j}_k^{\parallel}\}$ depend on the shape of the object, but are independent of the object material, and of the frequency of operation;
- ii the eigenvalues are real and positive;
- iii the eigenmodes are orthonormal according to the scalar product 1;

The eigenvalues of a spherical surface of unit radius have the analytical expression

$$\gamma_n^{\parallel} = \frac{n(n+1)}{(2n+1)} \quad n = 1, 2, 3, \dots \quad (5)$$

We now introduce a spherical coordinate system. The spherical coordinates of the point with position vector \mathbf{r} are (r, θ, ϕ) (with $0 \leq r < \infty$, $0 \leq \theta < \pi$ and $0 \leq \phi < 2\pi$). The basis for the three-dimensional vector space is the set $(\hat{\mathbf{r}}, \hat{\boldsymbol{\theta}}, \hat{\boldsymbol{\phi}})$, where $\hat{\mathbf{r}}$ is the radial unit vector, $\hat{\boldsymbol{\theta}}$ is the polar unit vector, and $\hat{\boldsymbol{\phi}}$ is the azimuthal unit vector. The eigenmodes corresponding to γ_n^{\parallel} are the vector spherical harmonics $\mathbf{W}_n^m(\theta, \phi)$ where m is an integer such that $-n \leq m \leq n$:

$$\mathbf{j}_{mn}^{\parallel} = \mathbf{W}_n^m = \hat{\mathbf{r}} \times \mathbf{X}_n^m = \frac{1}{\sqrt{n(n+1)}} \nabla Y_n^m. \quad (6)$$

The spherical harmonic $Y_n^m(\theta, \phi)$ of degree n and order m is given by

$$Y_n^m(\theta, \phi) = C_{mn} P_n^{|m|}(\cos \theta) e^{im\phi} \quad (7)$$

where $P_n^m(\cos \theta)$ is the associated Legendre polynomial of degree n and order m , and C_{mn} is a normalization coefficient. The spherical harmonics are orthogonal. We normalize them in such a way that

$$\int |Y_n^m(\theta, \phi)|^2 \, d\Omega = 1, \quad (8)$$

where $\int(\cdot) \, d\Omega = \int_0^\pi d\theta \sin \theta \int_0^{2\pi} d\phi(\cdot)$. The normalization coefficient C_{mn} is equal to

$$C_{mn} = \sqrt{\frac{2n+1}{4\pi} \frac{(n-m)!}{(n+m)!}}. \quad (9)$$

The degree n also determines the multipolar order of the vector spherical harmonics (e.g. $n = 1$ for a dipole, $n = 2$ for a quadrupole, etc.). Thus, Eq. 5 shows that longitudinal modes associated with larger eigenvalues γ_n^{\parallel} are characterized by higher multipolar order.

B. Transverse static modes

The transverse static surface current modes (called *transverse static modes* in the following for brevity) are non-trivial solutions of the eigenvalue problem:

$$\mathcal{T}_0^{\perp} \{ \mathbf{j}_k^{\perp} \} (\mathbf{r}) = \gamma_k^{\perp} \mathbf{j}_k^{\perp} \quad \text{on } \partial\Omega, \quad (10)$$

with

$$\mathcal{T}_0^{\perp} \{ \mathbf{w} \} (\mathbf{r}) = -\hat{\mathbf{n}} \times \hat{\mathbf{n}} \times \oint_{\partial\Omega} g_0(\mathbf{r} - \mathbf{r}') \mathbf{w}(\mathbf{r}') \, dS'. \quad (11)$$

Apart from a multiplicative factor, the integral operator 11 gives the static vector potential generated by a surface current distribution. Its spectrum has the following properties, that can be derived using the standard methods of eigenvalue problems, analogously to [27], [44]:

- i The eigenvalues $\{\gamma_k^\perp\}$ and the modes $\{\mathbf{j}_k^\perp\}$ depend on the shape of the object, and are independent of the object material and of the frequency of operation
- ii the eigenvalues are real and positive;
- iii the modes $\{\mathbf{j}_k^\perp\}$ associated are orthonormal according to the scalar product 1.

The eigenvalues of a spherical surface of unit radius have the analytical expression

$$\gamma_n^\perp = \frac{1}{(2n+1)} \quad n = 1, 2, 3, \dots \quad (12)$$

The modes corresponding to γ_n^\perp are the vector spherical harmonics $\mathbf{X}_n^m(\theta, \phi)$ where m is an integer such that $-n \leq m \leq n$:

$$\mathbf{j}_{mn}^\perp = \mathbf{X}_n^m = \frac{1}{\sqrt{n(n+1)}} \nabla Y_n^m \times \mathbf{r}. \quad (13)$$

The degree n also determines the multipolar order of the vector spherical harmonics (e.g. $n = 1$ for a dipole, $n = 2$ for a quadrupole, etc.). Thus, Eq. 12 shows that transverse modes associated with smaller eigenvalues γ_n^\perp are characterized by higher multipolar order.

C. Computation of the static modes

Let us introduce a surface triangulation of $\partial\Omega$, with N_p vertices, N_t elements, and N_e edges. We represent the static modes in term of convenient sub-domain basis functions, namely the loop and star functions [12], [45]. Specifically, any longitudinal mode \mathbf{j}_h^\parallel is expanded in terms of (non-solenoidal) star basis functions $\{\mathbf{j}_p^*\}$ with coefficients $\alpha_{h,p}^{\parallel*}$. Dually, any transverse mode \mathbf{j}_h^\perp is expanded in terms of (solenoidal) loop basis functions $\{\mathbf{j}_q^\circ\}$ with coefficients $\alpha_{h,q}^{\perp\circ}$:

$$\mathbf{j}_h^\parallel = \sum_{p=1}^{N_t-1} \alpha_{h,p}^{\parallel*} \mathbf{j}_p^*, \quad \mathbf{j}_h^\perp = \sum_{q=1}^{N_p-1} \alpha_{h,q}^{\perp\circ} \mathbf{j}_q^\circ. \quad (14)$$

The loop functions are divergence free, thus they correctly represent the transverse static modes. Instead, the star functions are not curl free (they are often denoted as quasi-curl [36]) thus they only approximately represent the longitudinal static modes. Both star and loop functions admit a linear representation in terms of RWG basis functions [8].

For closed surfaces with no handles, the number of linearly independent loop functions is $N_p - 1$, while the number of linearly independent star functions is $N_t - 1$. Thus, the numerical auxiliary eigenvalue problem for longitudinal static modes is

$$\mathbf{T}_0^{\parallel**} \mathbf{J}_h^* = \gamma_h^{\parallel} \mathbf{R}^{**} \mathbf{J}_h^*, \quad (15)$$

where $(\mathbf{T}_0^{\parallel**})_{pq} = \langle \mathbf{j}_p^*, \mathcal{T}_0^\parallel \mathbf{j}_q^* \rangle$, $(\mathbf{R}^{**})_{pq} = \langle \mathbf{j}_p^*, \mathbf{j}_q^* \rangle$, and $\mathbf{J}_h^* = [\alpha_{h,1}^{\parallel*}, \alpha_{h,2}^{\parallel*}, \dots, \alpha_{h,N_t-1}^{\parallel*}]^\top$. The numerical auxiliary eigenvalue problem for transverse static modes is

$$\mathbf{T}^{\perp\circ\circ} \mathbf{J}_h^\circ = \gamma_h^\perp \mathbf{R}^{\circ\circ} \mathbf{J}_h^\circ, \quad (16)$$

where $(\mathbf{T}^{\perp\circ\circ})_{pq} = \langle \mathbf{j}_p^\circ, \mathcal{T}_0^\perp \mathbf{j}_q^\circ \rangle$, $(\mathbf{R}^{\circ\circ})_{pq} = \langle \mathbf{j}_p^\circ, \mathbf{j}_q^\circ \rangle$, and $\mathbf{J}_h^\circ = [\alpha_{h,1}^{\perp\circ}, \alpha_{h,2}^{\perp\circ}, \dots, \alpha_{h,N_p-1}^{\perp\circ}]^\top$.

Since the loop and star functions are not orthogonal, the matrices \mathbf{R}^{**} and $\mathbf{R}^{\circ\circ}$ are not identity matrices, thus Eqs. 15 and 16 are *generalized* eigenvalue problems. The involved matrices are real, symmetric, and positive definite. Thus, efficient numerical algorithms for the eigenvalue calculation do apply, such as the Cholesky factorization [46]. Moreover, the matrices properties also determine the orthogonality, at the discrete level, of any pair of longitudinal modes, and any pair of transverse modes. The numerical integration of shape functions times the Green's functions or its gradient are evaluated using the techniques introduced by Graglia [47].

III. POGGIO-MILLER-CHANG-HARRINGTON-WU-TSAI (PMCHWT) SURFACE INTEGRAL EQUATION

A linear, homogeneous, isotropic material occupies the three-dimensional domain Ω . The material has permittivity $\varepsilon^+(\omega)$, permeability $\mu^+(\omega)$ and it is surrounded by a background medium with permittivity $\varepsilon^-(\omega)$ and permeability $\mu^-(\omega)$. The object is illuminated by a time harmonic electromagnetic field $\text{Re}\{\mathbf{E}_{inc}(\mathbf{r})e^{i\omega t}\}$. The equivalent electric \mathbf{j}_e and magnetic \mathbf{j}_m surface current densities, defined on $\partial\Omega$, are solutions of the following surface integral problem formulated by Poggio-Miller-Chang-Harrington-Wu-Tsai (PMCHWT) [38], [20], [39]:

$$\mathcal{Z} \mathbf{J} = \mathbf{F}, \quad (17)$$

where

$$\mathcal{Z} = \begin{pmatrix} \zeta^- \mathcal{T}_- + \zeta^+ \mathcal{T}_+ & \mathcal{K}_- + \mathcal{K}_+ \\ -(\mathcal{K}_- + \mathcal{K}_+) & \mathcal{T}_- / \zeta^- + \mathcal{T}_+ / \zeta^+ \end{pmatrix}, \quad (18)$$

$$\mathbf{J} = [\mathbf{j}_e, \mathbf{j}_m]^\top, \quad \mathbf{F} = [\mathbf{e}_0, \mathbf{h}_0]^\top, \quad (19)$$

$$\mathbf{e}_0 = -\hat{\mathbf{n}} \times \hat{\mathbf{n}} \times \mathbf{E}_{inc}|_{\partial\Omega}, \quad \mathbf{h}_0 = -\hat{\mathbf{n}} \times \hat{\mathbf{n}} \times \mathbf{H}_{inc}|_{\partial\Omega}. \quad (20)$$

The operators \mathcal{K}_\pm and \mathcal{T}_\pm are the MFIE and EFIE integral operators:

$$\mathcal{K}_\pm \{\mathbf{w}\}(\mathbf{r}) = \hat{\mathbf{n}} \times \hat{\mathbf{n}} \times \int_{\partial\Omega} \mathbf{w}(\mathbf{r}') \times \nabla' g^\pm(\mathbf{r} - \mathbf{r}') dS', \quad (21a)$$

$$\begin{aligned} \mathcal{T}_\pm \{\mathbf{w}\}(\mathbf{r}) &= jk^\pm \hat{\mathbf{n}} \times \hat{\mathbf{n}} \times \int_{\partial\Omega} g^\pm(\mathbf{r} - \mathbf{r}') \mathbf{w}(\mathbf{r}') dS' \\ &+ \frac{1}{jk^\pm} \hat{\mathbf{n}} \times \hat{\mathbf{n}} \times \int_{\partial\Omega} \nabla' g^\pm(\mathbf{r} - \mathbf{r}') \nabla'_S \cdot \mathbf{w}(\mathbf{r}') dS', \end{aligned} \quad (21b)$$

$\nabla'_S \cdot$ denotes the surface divergence, g^\pm is the homogeneous space Green's function of the region Ω_\pm , i.e.

$$g^\pm(\mathbf{r} - \mathbf{r}') = \frac{e^{-jk^\pm |\mathbf{r} - \mathbf{r}'|}}{4\pi |\mathbf{r} - \mathbf{r}'|}, \quad (22)$$

$k^\pm = \omega \sqrt{\mu^\pm \varepsilon^\pm}$, and $\zeta^\pm = \sqrt{\mu^\pm / \varepsilon^\pm}$.

A. Galerkin equations

Aiming at the solution of the PMCWHT equation 17, we represent the equivalent electric and magnetic surface currents in terms of the transverse static modes $\{\mathbf{j}_p^\perp\}_{p=1\dots N^\perp}$ associated with the first N^\perp eigenvalues γ_p^\perp (sorted in descending order), and in terms of the longitudinal static modes $\{\mathbf{j}_q^\parallel\}_{q=1\dots N^\parallel}$ associated with the first N^\parallel eigenvalues γ_q^\parallel (sorted in ascending order), namely

$$\begin{cases} \mathbf{j}_e(\mathbf{r}) \approx \sum_{p=1}^{N^\perp} \alpha_p^\perp \mathbf{j}_p^\perp(\mathbf{r}) + \sum_{q=1}^{N^\parallel} \alpha_q^\parallel \mathbf{j}_q^\parallel(\mathbf{r}), \\ \mathbf{j}_m(\mathbf{r}) \approx \sum_{p=1}^{N^\perp} \beta_p^\perp \mathbf{j}_p^\perp(\mathbf{r}) + \sum_{q=1}^{N^\parallel} \beta_q^\parallel \mathbf{j}_q^\parallel(\mathbf{r}). \end{cases} \quad (23)$$

The choice of sorting the longitudinal eigenvalues accordingly to an ascending order and the transverse eigenvalues accordingly to a descending order guarantees that low-index eigenvalues are associated with modes of low-order multipolar order (dipole, quadrupole, octupole ...).

Therefore, we define the unknown block vectors

$$\mathbf{J}_e = (\boldsymbol{\alpha}^\perp | \boldsymbol{\alpha}^\parallel)^\top, \quad \mathbf{J}_m = (\boldsymbol{\beta}^\perp | \boldsymbol{\beta}^\parallel)^\top, \quad (24)$$

with $\boldsymbol{\alpha}^a = [\alpha_1^a, \alpha_2^a, \dots, \alpha_{N^a}^a]^\top$ and with $\boldsymbol{\beta}^a = [\beta_1^a, \beta_2^a, \dots, \beta_{N^a}^a]^\top$ and $a = \parallel, \perp$.

We find the finite dimensional approximation of the PMCHWT problem by substituting Eq. 23 in Eq. 17 and by projecting along the same set of modes, accordingly to a Galerkin projection scheme:

$$\mathbf{Z}\mathbf{J} = \begin{pmatrix} \mathbf{E}_0 \\ \mathbf{H}_0 \end{pmatrix}, \quad (25)$$

where

$$\mathbf{J} = \begin{pmatrix} \mathbf{J}_e \\ \mathbf{J}_m \end{pmatrix}, \quad (26)$$

$$\mathbf{Z} = \begin{pmatrix} \zeta^- \mathbf{T}_- + \zeta^+ \mathbf{T}_+ & \mathbf{K}_- + \mathbf{K}_+ \\ -(\mathbf{K}_- + \mathbf{K}_+) & \mathbf{T}_- / \zeta^- + \mathbf{T}_+ / \zeta^+ \end{pmatrix}, \quad (27)$$

$$\mathbf{T}_\pm = \begin{pmatrix} \mathbf{T}_{\pm}^{\perp, \perp} & \mathbf{T}_{\pm}^{\perp, \parallel} \\ \mathbf{T}_{\pm}^{\parallel, \perp} & \mathbf{T}_{\pm}^{\parallel, \parallel} \end{pmatrix}, \quad \mathbf{K}_\pm = \begin{pmatrix} \mathbf{K}_{\pm}^{\perp, \perp} & \mathbf{K}_{\pm}^{\perp, \parallel} \\ \mathbf{K}_{\pm}^{\parallel, \perp} & \mathbf{K}_{\pm}^{\parallel, \parallel} \end{pmatrix}, \quad (28)$$

$$(\mathbf{K}_\pm^{ab})_{pq} = \langle \mathbf{j}_p^a | \mathbf{K}_\pm | \mathbf{j}_q^b \rangle, \quad (\mathbf{T}_\pm^{ab})_{pq} = \langle \mathbf{j}_p^a | \mathbf{T}_\pm | \mathbf{j}_q^b \rangle, \quad (29)$$

$$\mathbf{E}_0 = (\mathbf{E}_0^\perp | \mathbf{E}_0^\parallel)^\top, \quad \mathbf{H}_0 = (\mathbf{H}_0^\perp | \mathbf{H}_0^\parallel)^\top, \quad (30)$$

and

$$(\mathbf{E}_0^a)_p = \langle \mathbf{j}_p^a, \mathbf{e}_0 \rangle \quad (\mathbf{H}_0^a)_p = \langle \mathbf{j}_p^a, \mathbf{h}_0 \rangle, \quad (31)$$

with $a, b = \parallel, \perp$. The finite dimensional system has $2(N^\parallel + N^\perp)$ degrees of freedom.

We now decompose the Green's function as the sum of the static Green's function g_0 and a regular difference term $g_{d\pm}$:

$$g_\pm(\mathbf{r} - \mathbf{r}') = g_0(\mathbf{r} - \mathbf{r}') + g_{d\pm}(\mathbf{r} - \mathbf{r}'), \quad (32)$$

where

$$g_{d\pm}(\mathbf{r} - \mathbf{r}') = \frac{e^{-j\frac{k^\pm}{2}|\mathbf{r}-\mathbf{r}'|}}{4\pi j} k_\pm \text{sinc} \left\{ \frac{k^\pm}{2} |\mathbf{r} - \mathbf{r}'| \right\}. \quad (33)$$

In the past, the splitting of the Green's function into its static component and a difference term has been used to introduce well-conditioned and accurate scheme for the low-frequency analysis of PEC targets with the MFIE [48]. By applying this decomposition to the operators \mathcal{T}_\pm and \mathcal{K}_\pm , defined in 21a and 21b, we obtain:

$$\begin{aligned} \mathcal{T}_\pm &= +\frac{1}{jk^\pm} \mathcal{T}_0^\parallel - jk^\pm \mathcal{T}_0^\perp + \mathcal{T}_{d\pm}, \\ \mathcal{K}_\pm &= \mathcal{K}_0 + \mathcal{K}_{d\pm}, \end{aligned} \quad (34)$$

where \mathcal{T}_0^\parallel and \mathcal{T}_0^\perp are the static operators defined in Eqs. 3 and 11, and

$$\begin{aligned} \mathcal{T}_{d\pm} \{\mathbf{w}\}(\mathbf{r}) &= jk^\pm \hat{\mathbf{n}} \times \hat{\mathbf{n}} \times \int_{\partial\Omega} g_{d\pm}(\mathbf{r} - \mathbf{r}') \mathbf{w}(\mathbf{r}') dS' \\ &+ \frac{1}{jk^\pm} \hat{\mathbf{n}} \times \hat{\mathbf{n}} \times \int_{\partial\Omega} \nabla g_{d\pm}(\mathbf{r} - \mathbf{r}') \nabla'_S \cdot \mathbf{w}(\mathbf{r}') dS', \end{aligned} \quad (35)$$

$$\mathcal{K}_0 \{\mathbf{w}\}(\mathbf{r}) = \hat{\mathbf{n}} \times \hat{\mathbf{n}} \times \int_{\partial\Omega} \mathbf{w}(\mathbf{r}') \times \nabla' g_0(\mathbf{r} - \mathbf{r}') dS', \quad (36)$$

$$\mathcal{K}_{d\pm} \{\mathbf{w}\}(\mathbf{r}) = \hat{\mathbf{n}} \times \hat{\mathbf{n}} \times \int_{\partial\Omega} \mathbf{w}(\mathbf{r}') \times \nabla' g_{d\pm}(\mathbf{r} - \mathbf{r}') dS'. \quad (37)$$

The above decomposition considerably simplifies the calculation of the finite dimensional operators \mathbf{T}_\pm^{ab} with $a, b = \parallel, \perp$, which are obtained by projecting the operator \mathcal{T}_\pm along the longitudinal and transverse static modes because $\{\mathbf{j}_k^\parallel\}$ and $\{\mathbf{j}_k^\perp\}$ diagonalize the static operators \mathcal{T}_0^\perp and \mathcal{T}_0^\parallel :

$$\begin{aligned} (\mathbf{T}_\pm^\parallel)_{pq} &= \langle \mathbf{j}_p^\parallel, \mathcal{T}_\pm | \mathbf{j}_q^\parallel \rangle = \\ &\frac{\gamma_p^\parallel}{jk^\pm} \delta_{p,q} - jk^\pm \langle \mathbf{j}_p^\parallel, \mathcal{T}_0^\perp | \mathbf{j}_q^\parallel \rangle + \langle \mathbf{j}_p^\parallel, \mathcal{T}_{d\pm} | \mathbf{j}_q^\parallel \rangle, \end{aligned} \quad (38a)$$

$$(\mathbf{T}_\pm^\perp)_{pq} = \langle \mathbf{j}_p^\perp, \mathcal{T}_\pm | \mathbf{j}_q^\perp \rangle = \langle \mathbf{j}_p^\perp, \mathcal{T}_{d\pm} | \mathbf{j}_q^\perp \rangle, \quad (38b)$$

$$(\mathbf{T}_\pm^{\perp\perp})_{pq} = \langle \mathbf{j}_p^\perp, \mathcal{T}_\pm | \mathbf{j}_q^\perp \rangle = \langle \mathbf{j}_p^\perp, \mathcal{T}_{d\pm} | \mathbf{j}_q^\perp \rangle, \quad (38c)$$

$$(\mathbf{T}_\pm^{\perp\parallel})_{pq} = \langle \mathbf{j}_p^\perp, \mathcal{T}_\pm | \mathbf{j}_q^\parallel \rangle = -jk^\pm \gamma_h^\perp \delta_{p,q} + \langle \mathbf{j}_p^\perp, \mathcal{T}_{d\pm} | \mathbf{j}_q^\parallel \rangle, \quad (38d)$$

where $\delta_{p,q}$ is the Kronecker delta. We point out that the numerical computation of the terms $\langle \mathbf{j}_p^\parallel, \mathcal{T}_{d\pm} | \mathbf{j}_q^\perp \rangle$ is straightforward, since their kernels are regular functions. These terms are the only ones depending on the operating frequency. The decomposition of the Green's function into the sum of a static term and of a regular difference term relieves us from the task of computing almost all the integrals with (integrable) singularity, which usually results in longer computational time compared to their regular counterpart. There are however two exceptions: $\langle \mathbf{j}_p^\parallel, \mathcal{T}_0^\perp | \mathbf{j}_q^\parallel \rangle$ and $\langle \mathbf{j}_p^\perp, \mathcal{K}_0^\perp | \mathbf{j}_q^\perp \rangle$, $\forall a, b \in \perp, \parallel$. These terms are frequency-independent, thus when the calculation of the scattering response of an object for multiple frequencies of the exciting field is required, they can be conveniently precalculated and stored away, while only the regular terms must be calculated at any frequencies.

B. Low-frequency analysis

Surface integral formulations may suffer from ill-conditioning due to low frequency breakdown. The low frequency breakdown phenomenon manifests when the operating wavelength is much larger than the dimension of the object [49], and originates from the different frequency-scaling of the terms associated with the vector and the scalar potentials. This is a common scenario which may be encountered in several applications, including metamaterials and electromagnetic bandgap (EBG) structures, or in the analysis of interconnects and packaging. This problem has been addressed by using quasi-Helmholtz decompositions, such as loop/star [49], [45], [50], loop-tree [13], [51], or null-pinv [52] decomposition, followed by a basis rearrangement [53], [54]. It is also worth to point out that some formulations are immune from this problem, such as the N-Müller formulation [55], or the formulation obtained by augmenting the traditional EFIE by including charge as extra unknown [56], [57].

In this section, we summarize the behaviour of the PMCHWT at very low frequencies. In this limit, the frequency dependence of the elements of the matrix Z follows different scaling laws, which are easily determined by following [54], [58]

$$\begin{pmatrix} \mathbf{T}_{\pm}^{\perp\perp} & \mathbf{T}_{\pm}^{\parallel\perp} \\ \mathbf{T}_{\pm}^{\parallel\parallel} & \mathbf{T}_{\pm}^{\perp\parallel} \end{pmatrix} \xrightarrow{\omega \downarrow 0} \begin{pmatrix} -jk^{\pm}\Gamma^{\perp} & j(k^{\pm})^3\mathbf{T}_2^{\parallel\perp} \\ j(k^{\pm})^3\mathbf{T}_2^{\parallel\perp} & +\Gamma^{\parallel}/jk^{\pm} \end{pmatrix}, \quad (39)$$

$$\begin{pmatrix} \mathbf{K}_{\pm}^{\perp\perp} & \mathbf{K}_{\pm}^{\perp\parallel} \\ \mathbf{K}_{\pm}^{\parallel\perp} & \mathbf{K}_{\pm}^{\parallel\parallel} \end{pmatrix} \xrightarrow{\omega \downarrow 0} \begin{pmatrix} (k^{\pm})^2\mathbf{K}_2^{\perp\perp} & \mathbf{K}_0^{\perp\parallel} \\ \mathbf{K}_0^{\perp\parallel} & \mathbf{K}_0^{\parallel\parallel} \end{pmatrix}, \quad (40)$$

where Γ^{\perp} and Γ^{\parallel} are diagonal matrices, $\Gamma^{\perp} = \text{diag}\{\gamma_1^{\perp}, \gamma_2^{\perp}, \dots, \gamma_{N^{\perp}}^{\perp}\}$, $\Gamma^{\parallel} = \text{diag}\{\gamma_1^{\parallel}, \gamma_2^{\parallel}, \dots, \gamma_{N^{\parallel}}^{\parallel}\}$, and

$$\mathbf{T}_2^{\parallel\perp} = \frac{1}{8\pi} \int_{\partial\Omega} \mathbf{j}_p^{\perp}(\mathbf{r}) \cdot \int_{\partial\Omega} |\mathbf{r} - \mathbf{r}'| \mathbf{j}_q^{\perp}(\mathbf{r}') dS dS', \quad (41)$$

$$\mathbf{K}_2^{\perp\perp} = -\frac{1}{8\pi} \int_{\partial\Omega} \mathbf{j}_p^{\perp}(\mathbf{r}) \cdot \int_{\partial\Omega} \frac{(\mathbf{r} - \mathbf{r}')}{|\mathbf{r} - \mathbf{r}'|} \times \mathbf{j}_q^{\perp}(\mathbf{r}') dS dS'. \quad (42)$$

Thus, by using Eqs. 39 and 40 it easy to prove that, in the static limit, the discrete matrix Z approaches the matrix Z_0 which exhibits the following frequency dependence:

$$Z_0 \propto \begin{bmatrix} \mathcal{O}(\omega) & \mathcal{O}(\omega^3) & \mathcal{O}(\omega^2) & \mathcal{O}(1) \\ \mathcal{O}(\omega^3) & \mathcal{O}(\omega^{-1}) & \mathcal{O}(1) & \mathcal{O}(1) \\ \mathcal{O}(\omega^2) & \mathcal{O}(1) & \mathcal{O}(\omega) & \mathcal{O}(\omega^3) \\ \mathcal{O}(1) & \mathcal{O}(1) & \mathcal{O}(\omega^3) & \mathcal{O}(\omega^{-1}) \end{bmatrix} \quad (43)$$

The excitation vector associated with a plane wave exhibits the following dependencies [54]:

$$\left[E_0^{\perp}, E_0^{\parallel}, H_0^{\perp}, H_0^{\parallel} \right]^{\top} \propto [\mathcal{O}(\omega), \mathcal{O}(1), \mathcal{O}(\omega), \mathcal{O}(1)]^{\top}. \quad (44)$$

Following [54], we introduce the rearrangement and scaling of the basis

$$\tilde{Z} = D_1 Z D_2, \quad (45)$$

where $D_1 = \text{diag}\{k^{-1}\mathbf{I}_{N^{\perp}}, \mathbf{I}_{N^{\parallel}}, k^{-1}\mathbf{I}_{N^{\perp}}, \mathbf{I}_{N^{\parallel}}\}$, $D_2 = \text{diag}\{\mathbf{I}_{N^{\perp}}, ik_{-}\mathbf{I}_{N^{\parallel}}, \mathbf{I}_{N^{\perp}}, ik_{-}\mathbf{I}_{N^{\parallel}}\}$, $\mathbf{I}_{N^{\perp}}$ is the the $N^{\perp} \times N^{\perp}$ identity matrix, and $\mathbf{I}_{N^{\parallel}}$ is the $N^{\parallel} \times N^{\parallel}$ identity matrix. After the above rearrangement the matrix \tilde{Z} is well-behaved.

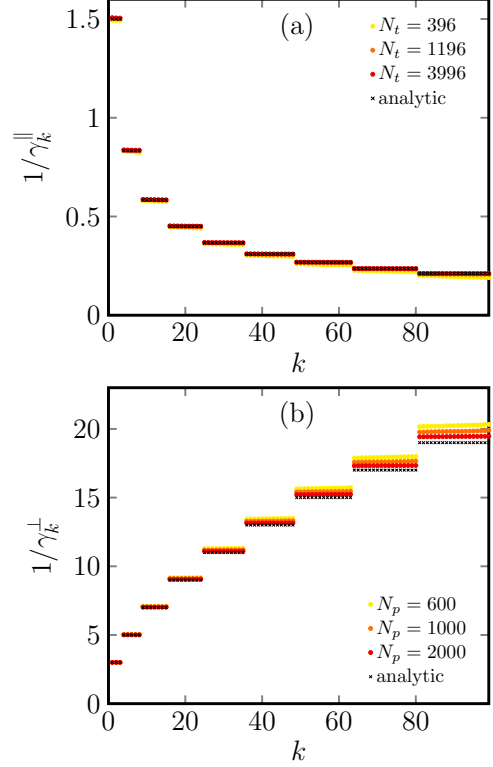


Fig. 1. Reciprocal of the first 100 eigenvalues γ_k^{\parallel} (a) and γ_k^{\perp} (b) associated with the longitudinal and transverse static modes of the sphere of unit radius. The eigenvalues are computed for several densities of the triangular surface mesh (filled circles of different colors) having N_t elements and N_p nodes and are compared with their analytical value.

IV. RESULTS AND DISCUSSION

The execution of the numerical algorithm can be subdivided into 4 stages: i) the assembly of the matrices \mathbf{T}_{\pm} , \mathbf{K}_{\pm} and of the vectors \mathbf{E}_0 , \mathbf{H}_0 in terms of loop/star basis functions; ii) the generation of the longitudinal/transverse static modes of an isolated object by solving the eigenvalue problems 15 and 16; iii) the ‘‘compression’’ stage, i.e. passing from the representation of the matrices \mathbf{T}_{\pm} , \mathbf{K}_{\pm} in terms of the loop/star basis to the representation in terms of the static modes basis. The compression does not need to be performed on the static part of the operators lying on the block-diagonal, since they are diagonalized by the static modes, as shown by Eqs. 38. iv) Direct matrix inversion using LU decomposition.

A. Sphere

We first consider the scattering from a sphere. This problem has an analytical solution [59], [17].

Figure 1 shows the convergence of the eigenvalues $\{\gamma_k^{\parallel}\}$ and $\{\gamma_k^{\perp}\}$ toward their analytical counterpart, given by Eqs. 5 and 12, as a function of the triangular mesh density. From now on, we consider the static basis calculated using a triangular mesh with $N_p = 1000$ nodes and $N_t = 1996$ triangles. The first 8 longitudinal modes are shown in Fig. 2, the first 8 transverse modes are shown in Fig. 3.

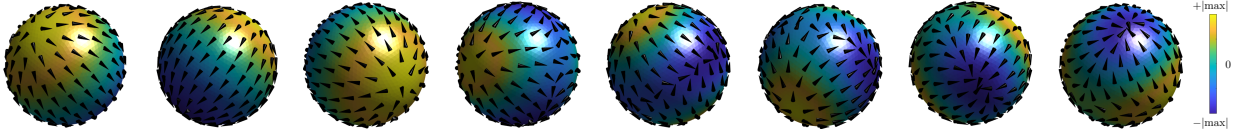


Fig. 2. Longitudinal static modes of a sphere. The modes are shown in lexicographic order, sorted (in ascending order) accordingly to their static eigenvalue. The first 8 modes are shown: the first three are associated to $n = 1$ (electric dipole) the next five to $n = 2$ (electric quadrupole). The arrows represent the direction of the surface current density field, the colors represent the surface charge density.

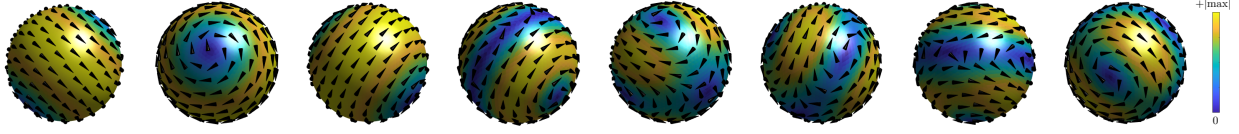


Fig. 3. Transverse static modes of a sphere. The modes are shown in lexicographic order, sorted (in descending order) accordingly to their static eigenvalue. The first 8 modes are shown: the first three are associated to $n = 1$ (magnetic dipole) the next five to $n = 2$ (magnetic quadrupole). The arrows represent the direction of the surface current density field, the colors represent the magnitude of the current density field.

In the discrete problem, the orthogonality between any pair of longitudinal modes and between any pair of transverse modes is always guaranteed, because the matrices $T^{\circ\circ}$ and T^{**} are real and symmetric. This property is indeed verified at the numerical level with machine precision. Instead, even if we expect that the mutual product between a transverse and a longitudinal static mode to be vanishing, this fact is only approximately verified, since the sub-domain basis functions used to represent the longitudinal modes, namely the “star” functions, are not rigorously curl-free [50]. Thus, it is worth calculating the “mutual” Gram matrix G , whose occurrences are defined as $g_{hk} = \langle \mathbf{j}_h^\perp, \mathbf{j}_k^\parallel \rangle$. The maximum occurrence of the mutual Gram matrix is 0.024 for a sphere with the considered surface mesh, assuming $\|\mathbf{j}_h^\parallel\| = \|\mathbf{j}_h^\perp\| = 1, \forall h$.

1) *Gold sphere:* We now use the static modes to solve the scattering problem from a gold sphere of radius $R = 100\text{nm}$ in the visible and near infrared spectral range. We describe the gold permittivity by interpolating experimental data [60]. At these frequencies, a metal nano-object may undergo plasmonic resonances, which have an electrostatic origin [25]. The sphere is excited by a linearly polarized plane wave of wavelength λ .

Figure 4 shows the scattering efficiency σ_{sca} as a function of λ . The scattering efficiency is defined as the scattering cross section normalized by the geometrical cross section G which, in this case, is $G = \pi R^2$ [17]. We consider different solutions, obtained by increasing the number of modes employed in the expansion 23, by keeping $N^\parallel = N^\perp$. The reference Mie solution [17] is also shown for comparison. For $N^\parallel = N^\perp = 5$, the numerical solution is in good agreement with the reference solution only in the long-wavelength regime, while it shows a slight disagreement when λ becomes comparable with R . Increasing the number of modes to $N^\parallel = N^\perp = 10$, we obtain a good agreement over the whole investigated spectrum. In this latter case, the inversion of a 40×40 matrix is required at each frequency.

In Fig. 5, we show the condition number of the PMCHWT problem with and without the rearrangement of the basis described in section III-B as a function of the sphere radius R , at $\lambda = 620\text{nm}$. It is apparent that, without the basis rearrangement, the condition number exponentially increases, which is

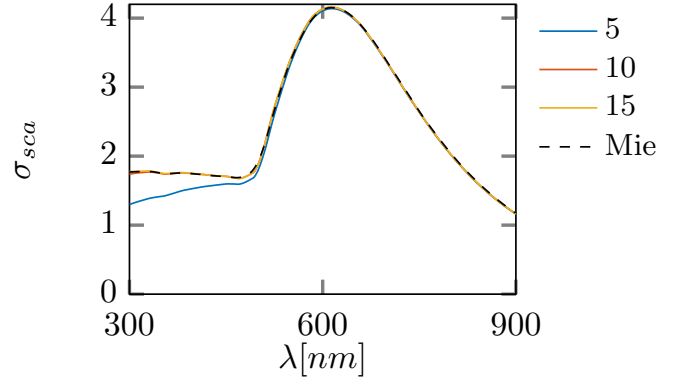


Fig. 4. Scattering efficiency σ_{sca} of a gold sphere with radius $R = 100\text{nm}$ excited by a linearly polarized plane wave at wavelength λ . σ_{sca} is evaluated using the PMCHWT and using an increasing number of longitudinal and transverse static modes ($N^\parallel = N^\perp = 5, 10, 15$). The reference Mie solution (black dashed line) is also shown for comparison.

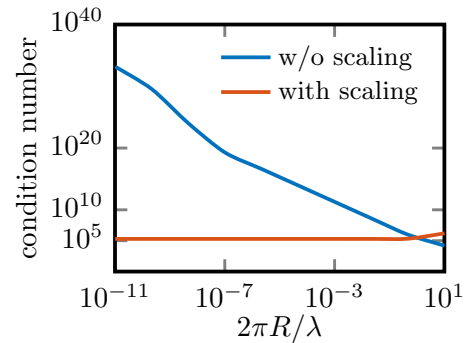


Fig. 5. Condition number with and without basis rearrangement and scaling, as a function of the size parameter $2\pi R/\lambda$, assuming $N^\parallel = N^\perp = 15$. We considered a gold sphere of varying radius R , excited by a linearly polarized plane wave at wavelength $\lambda = 620\text{nm}$.

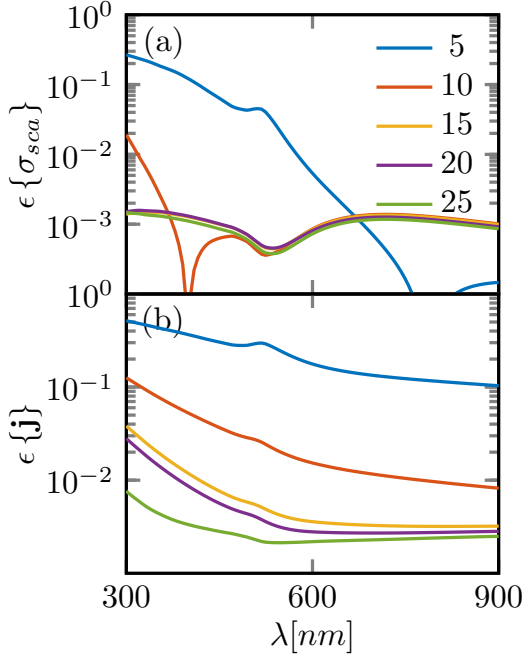


Fig. 6. Error made in the evaluation of the scattering efficiency $\epsilon[\sigma_{sca}]$ (a) and of the equivalent surface currents $\epsilon[\mathbf{j}]$ (b) of a gold sphere $R = 100\text{nm}$ by using $N^{\parallel} = N^{\perp} = 5, 10, 15, 25$ static modes (20, 40, 100 degrees of freedom). The reference loop/star solutions are obtained using 999 loop and 1996 star functions (5998 degrees of freedom). In both cases a PMCHWT formulation is used. The sphere is excited by a linearly polarized plane wave as a function of the wavelength λ .

symptomatic of the low-frequency breakdown problem. By rearranging the basis, the condition number is constant over the whole investigated range of R .

We now present a more systematic error analysis. In particular, we define the relative error on the scattering efficiency as

$$\epsilon[\sigma_{sca}] = |\sigma_{sca} - \tilde{\sigma}_{sca}| / \tilde{\sigma}_{sca}, \quad (46)$$

where $\tilde{\sigma}_{sca}$ is the reference solution which is obtained by solving the PMCHWT problem applying the finite element method with $N^{\circ} = 999$ loop functions and $N^{\star} = 1995$ star functions, associated with the same mesh used for the static modes generation. In Fig. 6 (a), we plot $\epsilon[\sigma_{sca}]$ as a function of the wavelength λ , by varying the number of static modes, keeping $N^{\parallel} = N^{\perp}$. We note that for $N^{\parallel} = N^{\perp} \geq 10$ the achieved error is lower than 0.002 all over the investigated spectral range. The error only slowly decrease if the number of modes $N^{\parallel} = N^{\perp}$ is increased from 15 to 25. Then, we investigate the error in the evaluation of the equivalent surface currents. They are immediately related to the total electric field on the surface of the object, which has a great importance in nano-optics applications [61]. We define the relative error as:

$$\epsilon[\mathbf{J}] = \|\mathbf{J} - \tilde{\mathbf{J}}\|_2 / \|\tilde{\mathbf{J}}\|_2, \quad (47)$$

where $\tilde{\mathbf{J}}$ is the reference loop/star solutions and $\|\cdot\|_2$ is the Euclidean norm. In Fig. 6 (b), we show $\epsilon[\mathbf{J}]$ as a function of λ . Compared to panel (a), it is apparent that more static basis functions are needed to achieve a prescribed error.

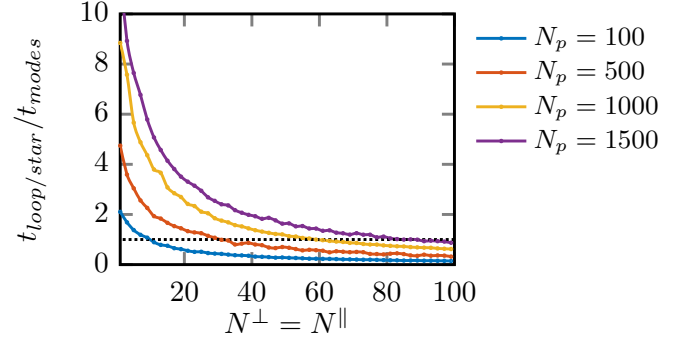


Fig. 7. Ratio between the total cpu time for the computation of the PMCHWT solution using the loop/star basis $t_{loop/star}$ and using the static mode basis t_{modes} . This ratio is evaluated as a function of the number of static modes $N^{\perp} = N^{\parallel}$ for different meshes with different number of nodes N_p , for the problem of scattering by a gold sphere excited by a plane wave with $\lambda = 620\text{nm}$.

We now analyze the cpu time required for the different stages of the numerical solution of the PMCHWT using static modes. The time spent by the algorithm for the matrix inversion using LU decomposition and for the static mode calculation is always negligible with respect to the time required for the assembly of the matrices \mathbf{K}_{\pm} and \mathbf{T}_{\pm} and for their compression. The compression is typically the most time consuming stage, and its cpu time increases linearly with the number of transverse/longitudinal modes employed. In Fig. 7, we show the ratio of the cpu-time $t_{loop/star}$ required to obtain the solution of the PMCHWT using the loop/star basis to the cpu-time t_{modes} required to obtain the solution using $N^{\perp} = N^{\parallel}$ static modes. This analysis is repeated for several mesh densities. The same mesh is used both for the calculation of the static modes and for the loop/star solution. For a surface mesh with $N_p = 100$ nodes, $t_{loop/star} > t_{modes}$ only when a few modes are used, namely $N^{\perp} = N^{\parallel} < 10$; for a number of modes larger than this threshold, the loop/star solution becomes faster. For denser meshes, the use of the static basis may become more favorable, while the condition $t_{loop/star} = t_{modes}$ is verified for a larger number of basis functions employed. For the mesh density used in the previous examples with $N_p = 1000$, the static mode solution is faster for $N^{\perp} = N^{\parallel} < 69$.

We now investigate the convergence of the static modes solution in the presence of an excitation located close to the object's surface. In Fig. 8, we consider an electric point dipole exciting a gold sphere of radius $R = 100\text{nm}$. The point dipole is placed at a distance of 30nm from the sphere's surface and oriented as sketched in the inset. We evaluate the total scattered power W_{sca} using an increasing number of longitudinal/transverse static modes ($N^{\parallel} = N^{\perp} = 5, 10, 15$). We also show the reference Mie solution (black dashed line) for comparison. As soon as $N^{\parallel} = N^{\perp} = 15$, the two solutions become indistinguishable.

In Fig. 9, we investigate the two relative errors $\epsilon[W_{sca}]$ and $\epsilon[\mathbf{j}]$, assuming the loop/star solution as reference. Figure 9 (a) shows that the total scattered power evaluated using the static modes quickly converges toward the loop/star solution, with a

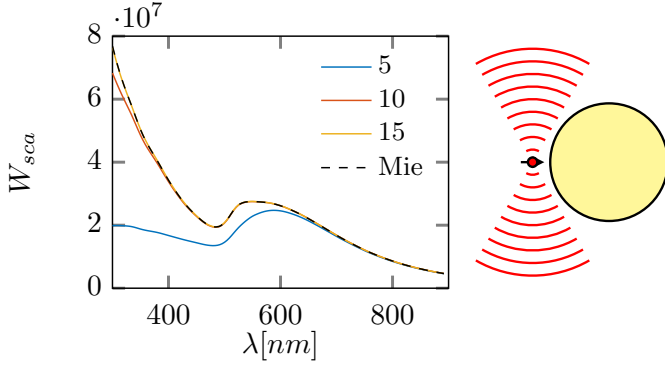


Fig. 8. Scattered power W_{sca} by a gold sphere with radius $R = 100\text{nm}$ excited by an electric point dipole, located at a distance of 30nm from the surface of the particle, and oriented as shown in the inset. W_{sca} is evaluated as a function of the wavelength λ using the PMCHWT and employing an increasing number of longitudinal/transverse static modes ($N^{\parallel} = N^{\perp} = 5, 10, 15$). The reference Mie solution (black dashed line) is also shown for comparison.

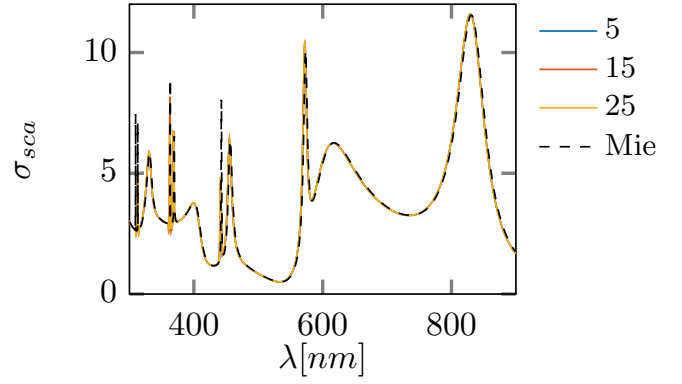


Fig. 10. Scattering efficiency σ_{sca} of a dielectric sphere with $R = 100\text{nm}$ and $\epsilon_R = 16$, excited by a linearly polarized plane wave evaluated by the PMCHWT with an increasing number of longitudinal and transverse static modes ($N^{\parallel} = N^{\perp} = 5, 10, 15$). The reference Mie solution (black dashed line) is also shown for comparison.

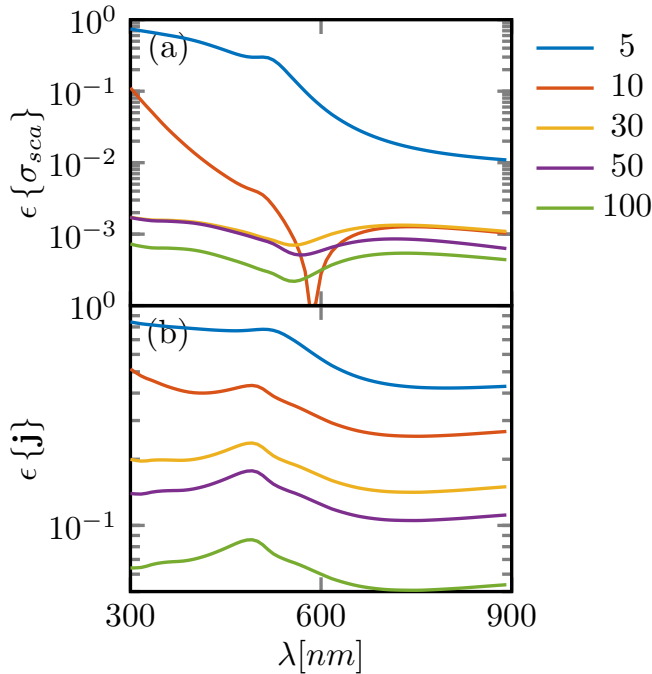


Fig. 9. Error made in the evaluation of the scattered power W_{sca} and of the equivalent surface currents $\epsilon\{j\}$ (b) of a gold sphere $R = 100\text{nm}$ by solving the PMCHWT using $N^{\parallel} = N^{\perp} = 5, 10, 30, 50, 100$ static modes. The reference quantities are obtained by solving the PMCHWT using 999 loop and 1996 star functions. The sphere is excited by a dipole, located at a distance of 30nm from the surface of the particle and oriented as shown in the inset of Fig. 8.

rate comparable to the one observed in Fig. 6 (a). Instead, the convergence of the surface currents is much slower because rapid spatial variations of the surface current in proximity of the exciting dipole require higher order static modes to be accurately described.

2) *High-permittivity sphere*: We now consider a high permittivity sphere, assumed to be non-dispersive in time with relative permittivity $\epsilon_R = 16$. Sub-wavelength objects of sufficiently high permittivity may support scattering resonances, which have a magnetostatic origin [27], [30].

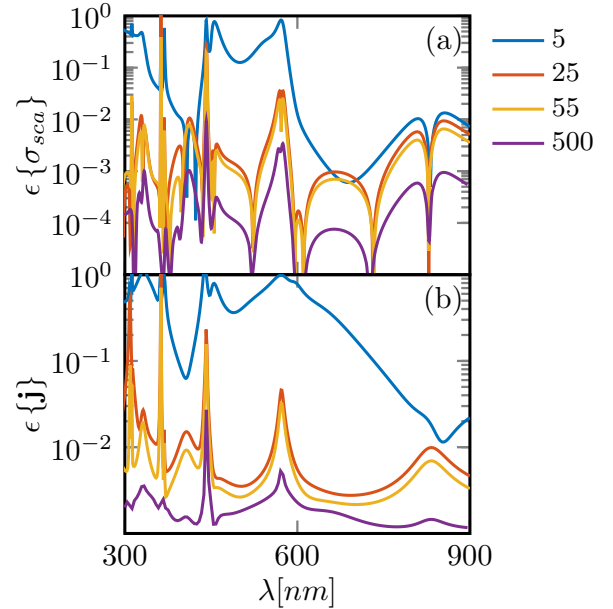


Fig. 11. Error made in the evaluation of the scattering efficiency σ_{sca} (a) and of the equivalent surface currents j (b) of a dielectric sphere with $\epsilon_R = 16$ and $R = 100\text{nm}$ by solving the PMCHWT equation using the static mode basis with $N^{\parallel} = N^{\perp} = 5, 25, 55, 500$. The reference values are obtained by solving the PMCHWT and using the loop/star expansion. The sphere is excited by a linearly polarized plane wave as a function of the wavelength λ .

In Fig. 10, we calculate the scattering efficiency σ_{sca} as a function of the wavelength of the exciting, linearly polarized, plane wave. We consider different solutions computed using an increasing number of modes, by keeping $N^{\parallel} = N^{\perp}$. We use as reference the analytic Mie solution [59], [17], shown with a black dashed line. Even if a good agreement is found at low frequency with $N^{\parallel} = N^{\perp} = 5$, the accuracy of the solution deteriorates at higher frequencies, and it is unable to describe some peaks of the scattering response. By increasing the number of employed modes to $N^{\parallel} = N^{\perp} = 10$, we obtain a very good agreement over the whole investigated spectrum.

We now quantify the errors in the scattering efficiency and in the surface currents of the static mode solution. In Fig.

11 (a), we plot $\epsilon[\sigma_{sca}]$ as a function of λ , employing an increasing number of modes with the constraint $N^\perp = N^\parallel$. When $N^\perp = N^\parallel = 5$, the error is acceptable as long λ is much larger than the dimension of the object, then the error suddenly increases for wavelengths below 600nm. By assuming $N^\perp = N^\parallel = 25$, we obtain a low error all over the investigated spectrum. Only at the resonances the error slightly exceeds 0.01. A further increase in the number of basis function improves the convergence, especially in the neighborhood of the resonance peaks. In order to check the convergence of the static mode expansion, we also considered $N^\perp = N^\parallel = 500$. We obtain errors which are less than 0.009 for the σ_{sca} and less than 0.03 for \mathbf{j} over the whole investigated spectral range.

B. Rod

We now consider a non-canonical shape, namely a three-dimensional rod. We model this shape as a superellipsoid, whose boundary has the implicit equation $(x/a)^r + (y/b)^r + (z/a)^r = 1$, with $b = 0.5a$, $c = 0.25a$, and $r = 6$. We used the public domain code developed by Per-Olof Persson and Gilbert Strang [62] to generate a surface mesh with 1000 nodes and 1996 triangular elements. The first 8 longitudinal and 8 transverse static modes are shown in Fig. 12 and 13, respectively.

1) *Gold rod*: First, we investigate a gold [60] rod with $a = 100\text{nm}$, excited by a plane wave linearly polarized along the direction $(\hat{x} + \hat{y})/\sqrt{2}$ and propagating along the \hat{z} axis. In Fig. 14 we plot the spectrum of the scattering efficiency σ_{sca} , obtained by increasing the number of modes $N^\perp = N^\parallel = 5, 10, 15$. We take as reference the loop/star solution, with 5984 total degrees of freedom. Only five longitudinal and transverse modes (20 total degrees of freedom) are sufficient to achieve a sufficiently good agreement with the reference solution over the whole investigated spectrum, demonstrating a drastic reduction of the total number of unknowns.

In Fig. 15, we perform a more systematic analysis of the error on the scattering cross section $\epsilon[\sigma_{sca}]$ (a), and on the equivalent surface currents $\epsilon[\mathbf{j}]$ (b). Overall, the errors are slightly higher than in the case of a sphere. Besides that, as in the previous numerical experiments, we conclude that i) the error on the surface currents are one order of magnitude higher than the error on the scattering efficiency, and ii) the rate of convergence is not uniform as a function of the number of employed modes, and becomes slower as $N^\parallel = N^\perp$ increases.

2) *High-permittivity Rod*: Here, we investigate a high-permittivity rod. The relative permittivity of the rod is assumed constant over the investigated frequency spectrum to the value $\epsilon_R = 16$. In Fig. 16, we plot the σ_{sca} spectrum, obtained by increasing the numbers of static modes employed. We use as reference the loop/star solution, with 5984 degrees of freedom. If the wavelength is much larger than the dimension of the rod, $N^\perp = N^\parallel = 15$ are enough to correctly describe the scattering cross section. Nevertheless, the accuracy is lost as soon as the wavelength becomes comparable to the linear dimensions of the rod and high-frequency resonance peaks are not correctly described. Only by increasing the number of modes $N^\perp = N^\parallel$

n	1	4	9	16	25
$\epsilon[\sigma_{sca}][\%]$	0.2	0.68	2.5	2.8	3.3
$\epsilon[\mathbf{j}_{sca}]$	2.0	3.3	3.4	3.5	3.4

TABLE I

ERRORS IN THE SOLUTION OF THE SCATTERING PROBLEM BY A PERIODIC ARRAY MADE BY n SPHERES.

to 55, all the resonance peaks, including the high-frequency ones, are correctly described.

Figure 17 offers a more quantitative analysis of the errors (a) $\epsilon[\sigma_{sca}]$, (b) $\epsilon[\mathbf{j}]$. We note that, while for large wavelength a number of modes $N^\perp = N^\parallel = 15$ is sufficient to have an error below $\epsilon[\sigma_{sca}] < 0.01$ and $\epsilon[\mathbf{j}] < 0.2$, if the wavelength becomes comparable to the rod largest dimension, as many as 55 longitudinal and transverse static modes are needed to contain the error. Even in this case, the accuracy is deteriorated in the neighborhood of the resonance peaks. In order to check the convergence of the static mode expansion, we also considered $N^\perp = N^\parallel = 500$. We obtain errors which are less than 0.0015 for the σ_{sca} and less than 0.0068 for \mathbf{j} over the whole investigated spectral range.

In conclusion, even if compared to the previously investigated scenarios, a higher number of modes is needed to correctly describe the unknown current densities, the number of modes needed to describe the solution still remains much smaller than the number of loop/star functions required to achieve a comparable accuracy.

C. Solution of Multiple Scattering Problems

The static mode basis finds its natural application in the numerical solution of multiple scattering problems, where an array, whose dimension can be much larger than the incident wavelength, is made of n objects with identical shape but with different orientation and size.

We support the above statement through several examples. Specifically, we consider a finite-size periodic array of n spheres, of radius $R = 100\text{nm}$, which are placed at the nodes of a $\sqrt{n} \times \sqrt{n}$ square grid of pitch 250nm. The values of pitch and radius also fix the edge-edge interparticle separation to 50 nm. The geometry of a 13×13 array of 169 spheres is shown in Fig. 18. The array is excited by a plane wave, linearly polarized in the plane of the array, along one of the two axis, and propagating in the direction orthogonal to the array's plane with wavelength $\lambda = 600\text{nm}$. Each sphere is described by a surface mesh having 200 nodes and 396 triangles and 594 edges, which corresponds to a maximum edge length of the mesh's triangles $\approx \lambda/17$. A loop/star description leads to $1188n$ unknowns. Instead, we considered N^\parallel longitudinal and $N^\perp = 10$ transverse modes to describe the electric and magnetic surface currents on each nanoparticle, which correspond to $40n$ unknowns (a reduction of more than one order of magnitude).

In Fig. 19, we show the cpu time (in seconds) of the different stages of the numerical solution of the scattering problem from the finite-size periodic array of spheres, as a function of the number n of spheres ($n = 1, 4, 9, 16, \dots, 169$). The FORTRAN code runs on a single cpu. The total computational time is always dominated by the compression time, which

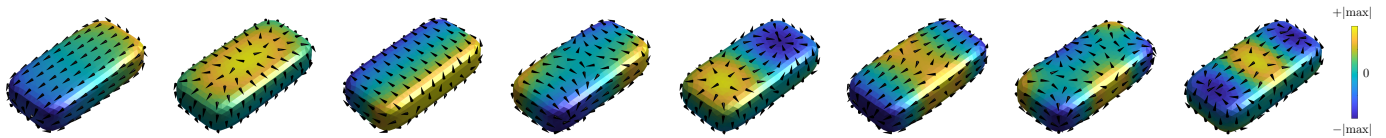


Fig. 12. Longitudinal static modes of a rod with semi-axis 1 : 0.5 : 0.25. The modes are shown in lexicographic order (ascending), sorted according to their static eigenvalue. The first 8 modes are shown. The arrows represent the direction of the surface current density field, the colors represent the surface charge density.

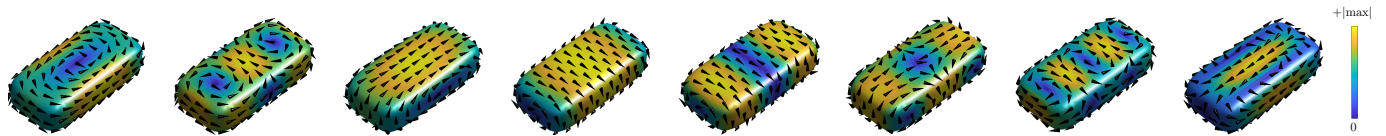


Fig. 13. Transverse static modes of a rod with semi-axis 1 : 0.5 : 0.25. The modes are shown in a lexicographic order (descending), sorted according to their static eigenvalue. The first 8 modes are shown. The arrows represent the direction of the surface current density field, the colors represent the magnitude of the current density field.

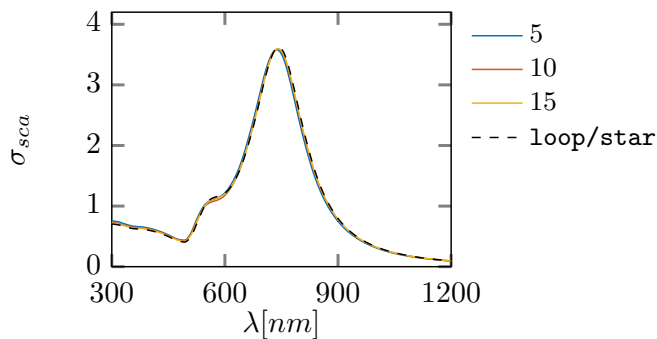


Fig. 14. Scattering efficiency σ_{sca} of a gold rod with semi-axis $a = 100nm$, $b = 0.5a$, and $c = 0.25a$ evaluated with an increasing number of longitudinal and transverse static modes $N^{\parallel} = N^{\perp} = 5, 15, 25, 35, 55$. The rod is excited by a linearly polarized plane wave. The reference loop/star solution (black dashed line) is also shown for comparison.

scales as $\propto n^2$. The assembly time, which also scales as $\propto n^2$, gives an important contribution to the total execution time. The time required for the computation of the static modes of the isolated sphere, which are used as basis, is negligible and it does not depend on the array's size. The inversion time, which scales as $\propto n^3$, is negligible if compared with the compression time, as in our case, if the dimensions of the arrays do not exceed a given number of particles (n_{th}). The value of n_{th} can be estimated extrapolating the the curves in Fig. 19, and it is $n_{th} \approx 80k$ particles.

In Fig. 20 we compare the total cpu-time required for the solution of the PMCHWT solution using the static modes basis against the corresponding time required to obtain the loop/star solution, as a function of n . For $n > 4$, the static mode solution becomes advantageous, and the speed up further increases as n increases. In Tab. I, we also compare for $n \leq 25$ the error made by the static mode solution compared to the loop/star reference: it is always less then 4% for both the scattering efficiency and the currents.

To obtain information on the scaling laws, we fit the total computational time of the solution of the PMCHWT in terms of the static basis using the curve $t = 3n^2$, and in terms of

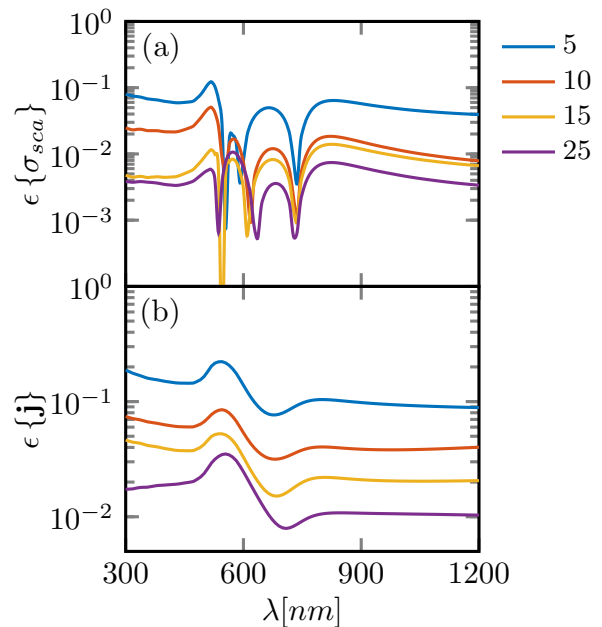


Fig. 15. Error ϵ in the evaluation of the scattering efficiency σ_{sca} and of the equivalent surface current density of a gold rod with semi-axis $a = 100nm$, $b = 0.5a$, and $c = 0.25a$ by solving the PMCHWT using the static mode basis with $N^{\parallel} = N^{\perp} = 5, 15, 20, 25$. The reference values are obtained by solving the PMCHWT using the loop/star expansion.

the loop/star solution using the curve $t = 0.92n^3$. The ratio is $0.3n$. Thus, for a 5×5 array, the cpu-time required to obtain the loop/star solution is 7.5 time larger than the cpu-time required for the static mode solution. For $n = 169$ we extrapolate that the static mode solution is $50 \times$ faster, but it was not possible to verify it experimentally, since the time expected to compute the loop/star solution was prohibitive.

In Fig. 18, we plot the magnitude of the total electric field on the surface of each sphere of the $n = 169$ sphere array. For this case $n = 169$, we consider 520 static modes. The corresponding loop/star description would require $200k$ unknowns.

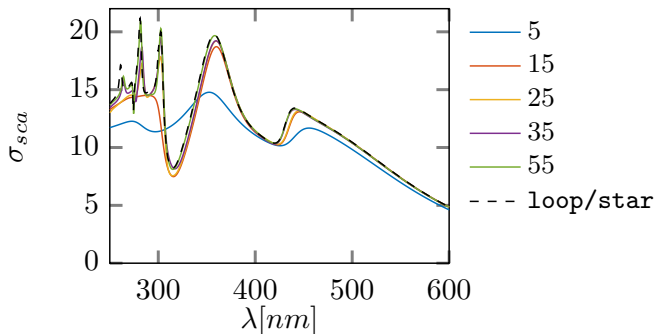


Fig. 16. Scattering efficiency σ_{sca} of a dielectric rod with $\epsilon_R = 16$ and semi-axis $a = 100nm$, $b = 0.5a$, and $c = 0.25a$ evaluated with an increasing number of longitudinal and transverse static modes $N^{\parallel} = N^{\perp} = 5, 15, 25, 35, 55$. The rod is excited by a linearly polarized plane wave. The reference loop/star solution (black dashed line) is also shown for comparison.

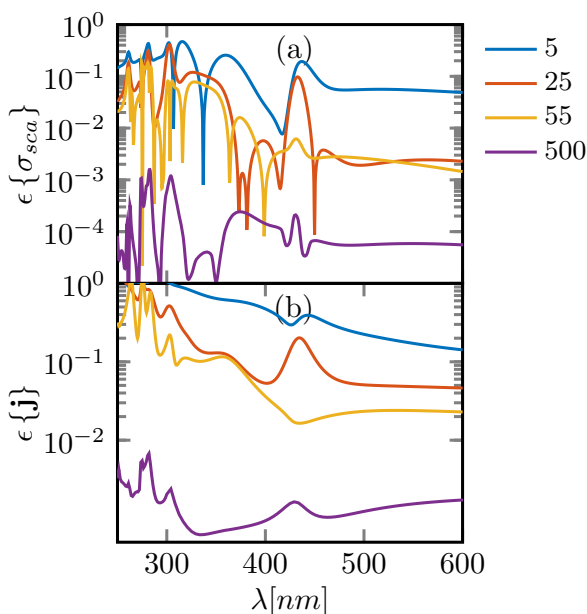


Fig. 17. Error ϵ in the evaluation of the scattering efficiency σ_{sca} and of the equivalent surface current density of a dielectric rod with $\epsilon_R = 16$ with semi-axis $a = 100nm$, $b = 0.5a$, and $c = 0.25a$ by solving the PMCHWT using an increasing number of longitudinal and transverse static modes $N^{\parallel} = N^{\perp} = 5, 25, 55, 500$. The reference values are obtained by solving the PMCHWT using the loop/star expansion.

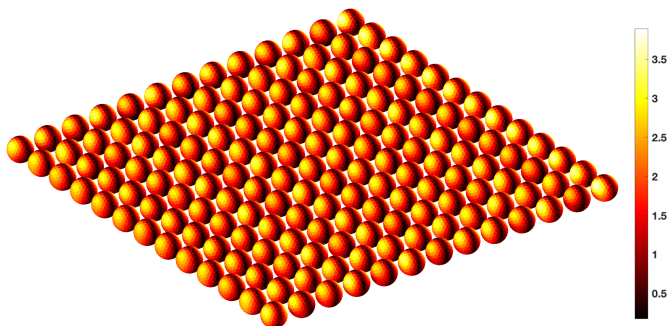


Fig. 18. Magnitude of the electric field on the particles' surface of a finite-size 13×13 periodic array of 169 gold spheres with radius $R = 100nm$ and edge-edge distance $50nm$. The edge of the array is $3.2\mu m$. The array is excited by a linearly polarized plane of wavelength $\lambda = 600nm$. The solution has been computed by using the static mode expansion with $N^{\parallel} = N^{\perp} = 10$.

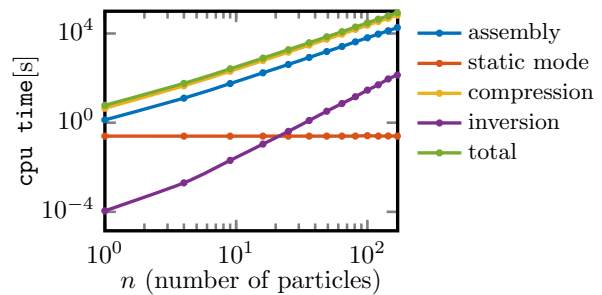


Fig. 19. CPU time (in seconds) of the different stages of the numerical solution of the scattering problem from an array of n spheres: Assembly of the matrices using the loop/star basis. Generation of the longitudinal/transverse static modes. Compression, by passing from loop/star to static modes. Direct inversion (LU). Total Time. The code is implemented in FORTRAN, and run on a single cpu.

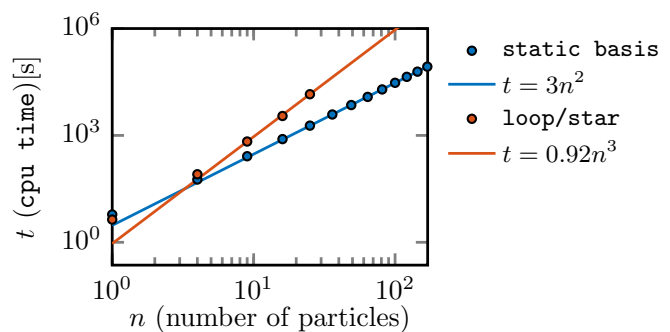


Fig. 20. Total execution CPU time (in seconds) of the numerical solution of the scattering problem from an array of n spheres by using loop/star basis functions and by using the static modes basis. Both codes are implemented in FORTRAN and run on a single cpu. The two fitting curves are shown with a continuous line.

V. CONCLUSIONS

We introduced a set of “static” surface current modes and used them to expand the unknown surface current densities in the surface integral equations governing the electromagnetic scattering problem from penetrable objects. We demonstrated the effectiveness of the static mode expansion in the solution of the Poggio-Miller-Chang-Harrington-Wu-Tsai (PMCHWT) formulation [38], [20], [39]. We found several characteristics that make the use of static modes appealing:

- The retarded Green’s function, constituting the kernel of integral operators recurring in surface integral formulations such as the PMCHWT, may be decomposed as the sum of the static Green’s function (with integrable singularity) and a proper difference (which is a regular function); the resulting integral operators containing the static Green’s function are diagonalized by the static modes, thus the overall problem is regularized [63].
- The use of the static mode expansion combined with an appropriate rescaling and rearranging of the unknowns makes the PMCHWT formulation immune from the low-frequency breakdown problem.
- The static modes only depend on the shape of the object, thus, the same static basis can be used (and has the same advantages) regardless of the operating frequency and

material of object. This fact enables the description of any scattering scenario involving one of more objects of a given shape, in terms of the same “alphabet” of basis functions, regardless of the frequency of operation. This fact constitutes an advantage compared to other basis sets (e.g., characteristic modes), where the modes depend on frequency and materials, thus the alphabet of basis functions, in which the scattering process is described, changes every time one of these parameters is varied, thus preventing a unified description.

As test cases, we considered the scattering from both metal and high-permittivity dielectric objects. We found that for objects of size smaller than the wavelength of operation, excited by a slowly varying electromagnetic field, only few modes are sufficient to accurately describe the emergent scattering response. Thus, the use of the static mode expansion drastically reduces the number of unknowns compared to a discretization in terms of loop/star or RWG functions, without deteriorating the accuracy of the solution.

The most time consuming stage of the PMCHWT numerical solution using static modes is typically the “compression” stage, which is the change of the basis used to represent the impedance matrix from the loop/star set to the static modes set. In the scattering problem from an isolated particle, the use of the static modes set is convenient in terms of total cpu-time, compared with the use of a loop/star set, only when few static modes are needed to correctly describe the surface currents. Instead, the use of the static modes is very convenient in multiple scattering problems from particle’s arrays made of n objects with identical shape but different orientation and size. Even for small arrays the solution in terms of static mode is faster than the solution in terms of loop/star, and this advantage linearly increases with the number of particles n .

In conclusions, the results presented in this paper may promote the use of the static basis in multiple scattering problems, including the numerical modeling of metasurfaces and metalens.

REFERENCES

- [1] R. E. Collin, *Antennas and Radiowave Propagation*. McGraw-Hill College, 1985. [Online]. Available: https://books.google.it/books/about/Antennas_and_Radiowave_Propagation.html?id=YHepAAAACAAJ&redir_esc=y
- [2] N. Yu and F. Capasso, “Flat optics with designer metasurfaces,” *Nature Materials*, vol. 13, no. 2, pp. 139–150, Feb. 2014, bandiera_abtest: a Cg_type: Nature Research Journals Number: 2 Primary_atype: Reviews Publisher: Nature Publishing Group Subject_term: Metamaterials Subject_term_id: metamaterials. [Online]. Available: <https://www.nature.com/articles/nmat3839>
- [3] M. Khorasaninejad, F. Aieta, P. Kanhaiya, M. A. Kats, P. Genevet, D. Rousso, and F. Capasso, “Achromatic Metasurface Lens at Telecommunication Wavelengths,” *Nano Letters*, vol. 15, no. 8, pp. 5358–5362, Aug. 2015. [Online]. Available: <https://doi.org/10.1021/acs.nanolett.5b01727>
- [4] W. C. Chew, J.-M. Jin, E. Michielssen, and J. Song, Eds., *Fast and Efficient Algorithms in Computational Electromagnetics*. Boston: Artech House, Jul. 2000.
- [5] O. M. Bucci and G. D. Massa, “Use of characteristic modes in multiple-scattering problems,” *Journal of Physics D: Applied Physics*, vol. 28, no. 11, p. 2235, Nov. 1995. [Online]. Available: <https://iopscience.iop.org/article/10.1088/0022-3727/28/11/003/meta>
- [6] G. Angiulli, G. Amendola, and G. D. Massa, “Characteristic Modes in Multiple Scattering by Conducting Cylinders of Arbitrary Shape,” *Electromagnetics*, vol. 18, no. 6, pp. 593–612, Nov. 1998, publisher: Taylor & Francis _eprint: <https://doi.org/10.1080/02726349808908615>. [Online]. Available: <https://doi.org/10.1080/02726349808908615>
- [7] A. Doicu, T. Wriedt, and Y. A. Eremin, *Light Scattering by Systems of Particles: Null-Field Method with Discrete Sources: Theory and Programs*, ser. Springer Series in Optical Sciences. Berlin Heidelberg: Springer-Verlag, 2006. [Online]. Available: <https://www.springer.com/gp/book/9783540336969>
- [8] S. Rao, D. Wilton, and A. Glisson, “Electromagnetic scattering by surfaces of arbitrary shape,” *IEEE Transactions on Antennas and Propagation*, vol. 30, no. 3, pp. 409–418, May 1982, conference Name: IEEE Transactions on Antennas and Propagation.
- [9] A. Bossavit, *Computational electromagnetism: variational formulations, complementarity, edge elements*. Academic Press, 1998.
- [10] R. Albanese and G. Rubinacci, “Integral formulation for 3D eddy-current computation using edge elements,” *IEE Proceedings A (Physical Science, Measurement and Instrumentation, Management and Education, Reviews)*, vol. 135, no. 7, pp. 457–462, 1988.
- [11] G. Rubinacci and A. Tamburrino, “A broadband volume integral formulation based on edge-elements for full-wave analysis of lossy interconnects,” *IEEE transactions on antennas and propagation*, vol. 54, no. 10, pp. 2977–2989, 2006.
- [12] D. Wilton, J. Lim, and S. Rao, “A novel technique to calculate the electromagnetic scattering by surfaces of arbitrary shape,” *URSI Radio Science Meeting*, p. 322, 1993.
- [13] W.-L. Wu, A. W. Glisson, and D. Kajfez, “A study of two numerical solution procedures for the electric field integral equation at low frequency,” *Applied Computational Electromagnetics Society Journal*, vol. 10, no. 3, pp. 69–80, 1995.
- [14] L. Trintinalia and H. Ling, “First Order Triangular Patch Basis Functions for Electromagnetic Scattering Analysis,” *Journal of Electromagnetic Waves and Applications*, vol. 15, no. 11, pp. 1521–1537, Jan. 2001, publisher: Taylor & Francis _eprint: <https://doi.org/10.1163/156939301X00085>. [Online]. Available: <https://doi.org/10.1163/156939301X00085>
- [15] A. Buffa and S. H. Christiansen, “A Dual Finite Element Complex on the Barycentric Refinement,” *Mathematics of Computation*, vol. 76, no. 260, pp. 1743–1769, 2007, publisher: American Mathematical Society. [Online]. Available: <https://www.jstor.org/stable/40234460>
- [16] R. Graglia, D. Wilton, and A. Peterson, “Higher order interpolatory vector bases for computational electromagnetics,” *IEEE Transactions on Antennas and Propagation*, vol. 45, no. 3, pp. 329–342, Mar. 1997, conference Name: IEEE Transactions on Antennas and Propagation.
- [17] C. F. Bohren and D. R. Huffman, *Absorption and Scattering of Light by Small Particles*. Wiley, 1998.
- [18] L.-W. Li, X.-K. Kang, and M.-S. Leong, *Spheroidal Wave Functions in Electromagnetic Theory*. John Wiley & Sons, Apr. 2004.
- [19] R. Garbacz, “Modal expansions for resonance scattering phenomena,” *Proceedings of the IEEE*, vol. 53, no. 8, pp. 856–864, 1965.
- [20] Y. Chang and R. Harrington, “A surface formulation for characteristic modes of material bodies,” *IEEE Transactions on Antennas and Propagation*, vol. 25, no. 6, pp. 789–795, Nov. 1977, conference Name: IEEE Transactions on Antennas and Propagation.
- [21] R. Harrington, J. Mautz, and Yu Chang, “Characteristic modes for dielectric and magnetic bodies,” *IEEE Transactions on Antennas and Propagation*, vol. 20, no. 2, pp. 194–198, Mar. 1972.
- [22] Y. Chen and C.-F. Wang, *Characteristic Modes: Theory and Applications in Antenna Engineering*. John Wiley & Sons, Jun. 2015, google-Books-ID: suobBgAAQBAJ.
- [23] M. Faenzi, G. Minatti, D. González-Ovejero, F. Caminita, E. Martini, C. Della Giovampaola, and S. Maci, “Metasurface Antennas: New Models, Applications and Realizations,” *Scientific Reports*, vol. 9, no. 1, p. 10178, Jul. 2019. [Online]. Available: <https://www.nature.com/articles/s41598-019-46522-z>
- [24] C. Forestiere, G. Gravina, G. Miano, M. Pascale, and R. Tricarico, “Electromagnetic modes and resonances of two-dimensional bodies,” *Physical Review B*, vol. 99, no. 15, p. 155423, Apr. 2019, publisher: American Physical Society. [Online]. Available: <https://link.aps.org/doi/10.1103/PhysRevB.99.155423>
- [25] I. D. Mayergoyz, D. R. Fredkin, and Z. Zhang, “Electrostatic (plasmon) resonances in nanoparticles,” *Phys. Rev. B*, vol. 72, no. 15, p. 155412, Oct. 2005. [Online]. Available: <https://link.aps.org/doi/10.1103/PhysRevB.72.155412>
- [26] G. Miano, G. Rubinacci, and A. Tamburrino, “Numerical Modeling for the Analysis of Plasmon Oscillations in Metallic Nanoparticles,” *IEEE*

- Transactions on Antennas and Propagation*, vol. 58, no. 9, pp. 2920–2933, 2010.
- [27] C. Forestiere, G. Miano, G. Rubinacci, M. Pascale, A. Tamburrino, R. Tricarico, and S. Ventre, “Magnetoquasistatic resonances of small dielectric objects,” *Phys. Rev. Research*, vol. 2, no. 1, p. 013158, Feb. 2020. [Online]. Available: <https://link.aps.org/doi/10.1103/PhysRevResearch.2.013158>
- [28] C. Forestiere, G. Miano, M. Pascale, and R. Tricarico, “Quantum theory of radiative decay rate and frequency shift of surface plasmon modes,” *Physical Review A*, vol. 102, no. 4, p. 043704, Oct. 2020, publisher: American Physical Society. [Online]. Available: <https://link.aps.org/doi/10.1103/PhysRevA.102.043704>
- [29] C. Forestiere and G. Miano, “Operative approach to quantum electrodynamicism in dispersive dielectric objects based on a polarization-mode expansion,” *Physical Review A*, vol. 106, no. 3, p. 033701, Sep. 2022, publisher: American Physical Society. [Online]. Available: <https://link.aps.org/doi/10.1103/PhysRevA.106.033701>
- [30] C. Forestiere, G. Miano, and G. Rubinacci, “Resonance frequency and radiative Q-factor of plasmonic and dielectric modes of small objects,” *Phys. Rev. Research*, vol. 2, no. 4, p. 043176, Nov. 2020. [Online]. Available: <https://link.aps.org/doi/10.1103/PhysRevResearch.2.043176>
- [31] C. Forestiere and G. Miano, “Time-domain formulation of electromagnetic scattering based on a polarization-mode expansion and the principle of least action,” *Physical Review A*, vol. 104, no. 1, p. 013512, Jul. 2021, publisher: American Physical Society. [Online]. Available: <https://link.aps.org/doi/10.1103/PhysRevA.104.013512>
- [32] E. Suter and J. R. Mosig, “A subdomain multilevel approach for the efficient MoM analysis of large planar antennas,” *Microwave and Optical Technology Letters*, vol. 26, no. 4, pp. 270–277, 2000
- [33] V. V. S. Prakash and R. Mittra, “Characteristic basis function method: A new technique for efficient solution of method of moments matrix equations,” *Microwave and Optical Technology Letters*, vol. 36, no. 2, pp. 95–100, 2003, _eprint: <https://onlinelibrary.wiley.com/doi/pdf/10.1002/mop.10685>. [Online]. Available: <https://onlinelibrary.wiley.com/doi/abs/10.1002/mop.10685>
- [34] L. Matekovits, V. A. Laza, and G. Vecchi, “Analysis of Large Complex Structures With the Synthetic-Functions Approach,” *IEEE Transactions on Antennas and Propagation*, vol. 55, no. 9, pp. 2509–2521, Sep. 2007, conference Name: IEEE Transactions on Antennas and Propagation.
- [35] A. Freni, P. De Vita, P. Pirinoli, L. Matekovits, and G. Vecchi, “Fast-Factorization Acceleration of MoM Compressive Domain-Decomposition,” *IEEE Transactions on Antennas and Propagation*, vol. 59, no. 12, pp. 4588–4599, Dec. 2011, conference Name: IEEE Transactions on Antennas and Propagation.
- [36] G. Vecchi, L. Matekovits, P. Pirinoli, and M. Orefice, “Hybrid spectral-spatial method for the analysis of printed antennas,” *Radio Science*, vol. 31, no. 5, pp. 1263–1270, Sep. 1996, conference Name: Radio Science.
- [37] —, “A numerical regularization of the EFIE for three-dimensional planar structures in layered media (invited article),” *International Journal of Microwave and Millimeter-Wave Computer-Aided Engineering*, vol. 7, no. 6, pp. 410–431, 1997
- [38] T.-K. Wu and L. L. Tsai, “Scattering from arbitrarily-shaped lossy dielectric bodies of revolution,” *Radio Science*, vol. 12, no. 5, pp. 709–718, 1977
- [39] A. J. Poggio and E. K. Miller, “CHAPTER 4 - Integral Equation Solutions of Three-dimensional Scattering Problems,” in *Computer Techniques for Electromagnetics*, ser. International Series of Monographs in Electrical Engineering, R. Mittra, Ed. Pergamon, Jan. 1973, pp. 159–264.
- [40] R. F. Harrington, *Field computation by moment methods*. Wiley-IEEE Press, 1993.
- [41] P. Monk and D. o. M. S. P. M. PH, *Finite Element Methods for Maxwell's Equations*. Clarendon Press, Apr. 2003.
- [42] R. Scharstein, “Helmholtz decomposition of surface electric current in electromagnetic scattering problems,” in *[1991 Proceedings] The Twenty-Third Southeastern Symposium on System Theory*, Mar. 1991, pp. 424–426, ISSN: 0094-2898.
- [43] N. V. Nair and B. Shanker, “Generalized Method of Moments: A Novel Discretization Technique for Integral Equations,” *IEEE Transactions on Antennas and Propagation*, vol. 59, no. 6, pp. 2280–2293, Jun. 2011, conference Name: IEEE Transactions on Antennas and Propagation.
- [44] A. Tamburrino, G. Piscitelli, and Z. Zhou, “The monotonicity principle for magnetic induction tomography,” *Inverse Problems*, vol. 37, no. 9, p. 095003, Aug. 2021.
- [45] M. Burton and S. Kashyap, “A study of a recent, moment-method algorithm that is accurate to very low frequencies,” *Applied Computational Electromagnetics Society Journal*, vol. 10, pp. 58–68, 1995, publisher: APPLIED COMPUTATIONAL ELECTROMAGNETICS SOCIETY INC.
- [46] H. Golub and C. F. V. Loan, *Matrix Computations*. Baltimore, MD: Johns Hopkins University Press, 1983.
- [47] R. Graglia, “On the numerical integration of the linear shape functions times the 3-D Green’s function or its gradient on a plane triangle,” *Antennas and Propagation, IEEE Transactions on*, vol. 41, no. 10, pp. 1448–1455, Oct. 1993.
- [48] E. Ubeda and J. M. Rius, “Divergence-conforming discretization of second-kind integral equations for the RCS computation in the Rayleigh frequency region,” *Radio Science*, vol. 46, no. 05, pp. 1–10, Oct. 2011, conference Name: Radio Science.
- [49] D. R. Wilton and A. W. Glisson, “On improving the electric field integral equation at low frequencies,” Los Angeles, CA, Jun. 1981, pp. 22–24.
- [50] G. Vecchi, “Loop-star decomposition of basis functions in the discretization of the EFIE,” *IEEE Transactions on Antennas and Propagation*, vol. 47, no. 2, pp. 339–346, Feb. 1999, conference Name: IEEE Transactions on Antennas and Propagation.
- [51] F. P. Andriulli, “Loop-Star and Loop-Tree Decompositions: Analysis and Efficient Algorithms,” *IEEE Transactions on Antennas and Propagation*, vol. 60, no. 5, pp. 2347–2356, May 2012, conference Name: IEEE Transactions on Antennas and Propagation.
- [52] G. Miano and F. Villone, “A surface integral formulation of Maxwell equations for topologically complex conducting domains,” *IEEE Transactions on Antennas and Propagation*, vol. 53, no. 12, pp. 4001–4014, Dec. 2005, conference Name: IEEE Transactions on Antennas and Propagation.
- [53] J.-S. Zhao and W. C. Chew, “Integral equation solution of Maxwell’s equations from zero frequency to microwave frequencies,” *IEEE Transactions on Antennas and Propagation*, vol. 48, no. 10, pp. 1635–1645, Oct. 2000, conference Name: IEEE Transactions on Antennas and Propagation.
- [54] S. Chen, W. C. Chew, J. Song, and J.-S. Zhao, “Analysis of low frequency scattering from penetrable scatterers,” *IEEE Transactions on Geoscience and Remote Sensing*, vol. 39, no. 4, pp. 726–735, Apr. 2001, conference Name: IEEE Transactions on Geoscience and Remote Sensing.
- [55] P. Ylä-Oijala, H. Wallén, D. C. Tzarouchis, and A. Sihvola, “Surface Integral Equation-Based Characteristic Mode Formulation for Penetrable Bodies,” *IEEE Transactions on Antennas and Propagation*, vol. 66, no. 7, pp. 3532–3539, Jul. 2018, conference Name: IEEE Transactions on Antennas and Propagation.
- [56] M. Taskinen and P. Ylä-Oijala, “Current and charge Integral equation formulation,” *IEEE Transactions on Antennas and Propagation*, vol. 54, no. 1, pp. 58–67, Jan. 2006, conference Name: IEEE Transactions on Antennas and Propagation.
- [57] Z. G. Qian and W. C. Chew, “An augmented electric field integral equation for high-speed interconnect analysis,” *Microwave and Optical Technology Letters*, vol. 50, no. 10, pp. 2658–2662, 2008, _eprint: <https://onlinelibrary.wiley.com/doi/pdf/10.1002/mop.23736>. [Online]. Available: <https://onlinelibrary.wiley.com/doi/abs/10.1002/mop.23736>
- [58] C. Forestiere, G. Miano, G. Rubinacci, A. Tamburrino, L. Udpá, and S. Ventre, “A Frequency Stable Volume Integral Equation Method for Anisotropic Scatterers,” *IEEE Transactions on Antennas and Propagation*, vol. 65, no. 3, pp. 1224–1235, Mar. 2017.
- [59] G. Mie, “Beiträge zur Optik trüber Medien, speziell kolloidaler Metallösungen,” *Annalen der physik*, vol. 330, no. 3, pp. 377–445, 1908.
- [60] P. B. Johnson and R. W. Christy, “Optical Constants of the Noble Metals,” *Phys. Rev. B*, vol. 6, no. 12, pp. 4370–4379, Dec. 1972. [Online]. Available: <https://link.aps.org/doi/10.1103/PhysRevB.6.4370>
- [61] J. A. Schuller, E. S. Barnard, W. Cai, Y. C. Jun, J. S. White, and M. L. Brongersma, “Plasmonics for extreme light concentration and manipulation,” *Nat. Mater.*, vol. 9, pp. 193–204, 2010.
- [62] P.-O. Persson and G. Strang, “A Simple Mesh Generator in Matlab,” *SIAM Review*, vol. 46, no. 2, pp. 329–345, 2004, publisher: Society for Industrial and Applied Mathematics. [Online]. Available: <https://www.jstor.org/stable/20453511>
- [63] A. Nosich, “The method of analytical regularization in wave-scattering and eigenvalue problems: foundations and review of solutions,” *IEEE Antennas and Propagation Magazine*, vol. 41, no. 3, pp. 34–49, Jun. 1999, conference Name: IEEE Antennas and Propagation Magazine.